

# We are IntechOpen, the world's leading publisher of Open Access books Built by scientists, for scientists

6,900

Open access books available

186,000

International authors and editors

200M

Downloads

Our authors are among the

154

Countries delivered to

TOP 1%

most cited scientists

12.2%

Contributors from top 500 universities



WEB OF SCIENCE™

Selection of our books indexed in the Book Citation Index  
in Web of Science™ Core Collection (BKCI)

Interested in publishing with us?  
Contact [book.department@intechopen.com](mailto:book.department@intechopen.com)

Numbers displayed above are based on latest data collected.  
For more information visit [www.intechopen.com](http://www.intechopen.com)



# Experimental and Simulation Studies of the Primary and Secondary Vacuum Freeze Drying at Microwave Heating

Józef Nastaj and Konrad Witkiewicz  
*West Pomeranian University of Technology, Szczecin  
Poland*

## 1. Introduction

Freeze drying (FD) is a dehydration method used to obtain high-quality products, mainly foodstuffs, biomaterials, pharmaceuticals and other thermolabile materials. Compared with standard methods, the freeze drying technique ensures retaining original shape, color and texture of the product as well as the preservation of its flavor, nutritive content and biological activity. However, FD is an expensive and lengthy dehydration process carried out in three stages: pre-freezing, primary drying when ice sublimation takes place under vacuum, followed by desorption of residual, unfreezable bounded water during the secondary stage.

Material must be first cooled below its triple point to obtain frozen state. In the case of food and biomaterials freezing is done rapidly at temperature between  $-50^{\circ}\text{C}$  and  $-80^{\circ}\text{C}$ , below eutectic point to avoid destruction of cell walls by ice crystals. During the primary FD stage, the frozen water in dried material pores sublimates from the ice front, diffuses throughout the dried layer to the sample surface and next deposits on the condenser surface. The sublimation of water takes place in the range of temperature and pressure below the triple point (for water 273.16 K and 611.73 Pa, respectively). After primary drying, residual moisture content may be as high as 7%. Secondary drying is intended to reduce this to an optimum value for material stability - usually with moisture content between 0.5 and 2.0%. The typical freeze-dried products have a porous, nonshrunken structure resulted from structural rigidity achieved by frozen water and can be therefore easily rehydrated.

The use of conventional FD on industrial scale is restricted to rather high-value products. Recent research is being focused on reducing operating costs of FD by intensifying heat and mass transfer in dried material. Proposed various heating methods, cycled pressure strategies and formulated optimal control policies are limited by temperature constraints (Liapis & Bruttini, 2006). They must be set to avoid ice melting and scorching of exposed dried material layer. The major difficulty of process optimization results from the fact that imposed thermal gradient has direction opposite to vapor concentration gradient. Moreover, dried layer acts as a thermal insulation for heat fluxes being transferred toward frozen layer. New FD method that overcomes these disadvantages is microwave freeze drying (MFD). Microwaves penetrate very well into ice and supply energy for sublimation volumetrically and selectively, bypassing the problem of heat transport through the dried layer of the

material. Microwaves can heat without the aid of thermal gradients what has a positive effect on product quality. With recent development in microwave hardware, the cost of MFD equipment is currently not too high what makes this method a promising alternative to conventional technologies.

Although MFD can greatly improve the drying rate, there are still many problems to be resolved in the practice. Application of microwave heating is limited because of difficulty to control the final product quality. Therefore constraints should be set to avoid specific problems of MFD such as corona discharge and non-uniform heating, which cause ice melting and overheating. To analyze and overcome these problems the experimental and theoretical studies should be performed to obtain optimal control policy of MFD in relation to particular material being dried.

Applying microwave energy in the MFD process may cause appearance of plasma discharge in the vacuum chamber. This phenomenon happens when the electric field intensity  $E$  is above the threshold value what may seriously damage the final product. Therefore upper limit on the electric field strength should be set and taken into account in mathematical modeling.

When microwaves, usually at standard frequency  $f=2.45$  GHz, are applied in MFD, electric field strength  $E$  is the controllable process parameter which reflects heating intensity. The distribution of electric field strength in the microwave applicator and within the dried sample can be determined by solving Maxwell's equations. Such approach is mathematically difficult to apply and especially complicated for multimode applicators. Another difficulty results from the fact that the freeze-dried material consists of two layers: the frozen and the dried one, which are distinct dielectrics.

The exponential decay of the electric field intensity in a dielectric described by Lambert's law is usually omitted in MFD and simplified by the electric field strength value averaged for the whole material sample (Ma & Peltre, 1975a, 1975b; Péré et al., 2001; Schiffmann, 2006). Typical biomaterials and foodstuffs containing water in a frozen form as well as dried are characterized by extreme high penetration depth in order of few or even dozens of meters. For this reason the electric field strength distribution in the product formed as a thin layer or placed in vials is negligible.

For specific microwave system of constant frequency  $f$ , the efficiency of microwave energy absorption and dissipation into heat in the frozen and dried material layers depends on its dielectric properties: relative dielectric constant  $\epsilon'$  and relative loss factor  $\epsilon''$ . Both parameters vary with temperature therefore this dependency should be taken into consideration in the modelling for both sample regions.

Application of the microwave energy in MFD has been studied since the mid-20th century. The mathematical models of the MFD process are usually formulated with pseudo steady state assumption, and derived on the basis of heat and mass transfer analysis. Ma and Peltre in the 1975 described one of the first comprehensive mathematical models of the MFD of foodstuff. They obtained good agreement with experimental results of raw beef drying. Some researchers took into consideration the sublimation-condensation phenomena in MFD process (Liapis & Bruttini, 2006; Wang & Shi, 1998). Many mathematical analyses presented in papers concerning freeze drying at conventional heating can be adapted in the modeling of MFD after including the volumetric heat source term in model equations set (Liapis & Bruttini, 1996).

In this chapter the main ideas in MFD modeling are presented and key mechanisms of heat and mass transport governing the process are explained. The complex mathematical model

of the primary and secondary FD stages at microwave heating is formulated to derive optimal control policy of the process depending on thermophysical properties and thickness of material being dried, total pressure and input microwave power. One-dimensional two-region model of the primary MFD was developed and then solved using various numerical approaches such as Landau's transformation (LT) and Variable Time-Step (VTS) methods. Varying during the process sublimation front temperature caused by varying with time vapor diffusional mass transfer resistances was taken into account. Some of the simulated drying curves were compared with experimental results giving fairly good agreement. The mathematical model of the secondary MFD was also developed and solved using the Numerical Method of Lines (NMOL). Pressure drop in the material was taken into account and calculated using Ergun equation. As a result of the both models solution, the moisture contents and the temperature distributions in drying material were obtained. The analysis performed basing on mathematical modeling enables computation of optimal ranges of significant material and process parameters, which ensure obtaining good product quality and optimal MFD drying times.

## 2. Experimental

### 2.1 MFD equipment

Experimental investigations of the primary freeze drying of random solids at microwave heating were performed by means of the set-up composed of the microwave circuit, the vacuum system, the refrigeration system, the temperature and weight measurements devices and the data acquisition system (Fig. 1).

A cylindrical Teflon container filled with material to be dried is hanged on the extensometer balance inside the vacuum chamber. Temperature of dried material is measured by the fluoroptic thermometer (FOT Lab Kit - Luxtron Corp.). A probe with a phosphorus sensor inserted to the sample is connected by optical fiber, via vacuum feedthrough with module m600 outside the chamber. The module emits photon pulses towards sensor and simultaneously records the decay of returning fluorescence signal which varies with material temperature. On this basis the module estimates measured temperature with a maximum absolute accuracy of 0.1°C. The fluoroptic thermometer essentially does not interfere with electromagnetic field in the applicator and is transparent for microwaves.

Temperature inside the chamber is controlled by the refrigeration system with a refrigerant circulating in the vacuum chamber's jacket. Sublimated vapors are removed from the chamber by the cold trap cooled by means of liquid nitrogen. The vacuum pump is operating constantly whilst self-regulated purge valve maintains pressure in the vacuum chamber at the level of 100 Pa.

Generated microwaves of 2450 MHz frequency are transmitted via the waveguide, the coaxial cable, the directional coupler and the vacuum feedthrough to the applicator inside the vacuum chamber. Microwave power reflected in the applicator returns to the directional coupler which directs it to the dummy load where is totally dissipated. The sample is inserted into the microwave applicator which is constructed as a section of rectangular brazen waveguide and acts as a mono-modal resonant cavity (Fig. 2). One of applicator walls is the movable tuner and its position can be adjusted remotely by stepping motor. Microwave is transmitted via the coaxial cable to the type N connector coupled with the antenna. Electromagnetic wave propagates inside the applicator in  $TE_{01n}$  mode where  $n$  is the number of half wavelengths.

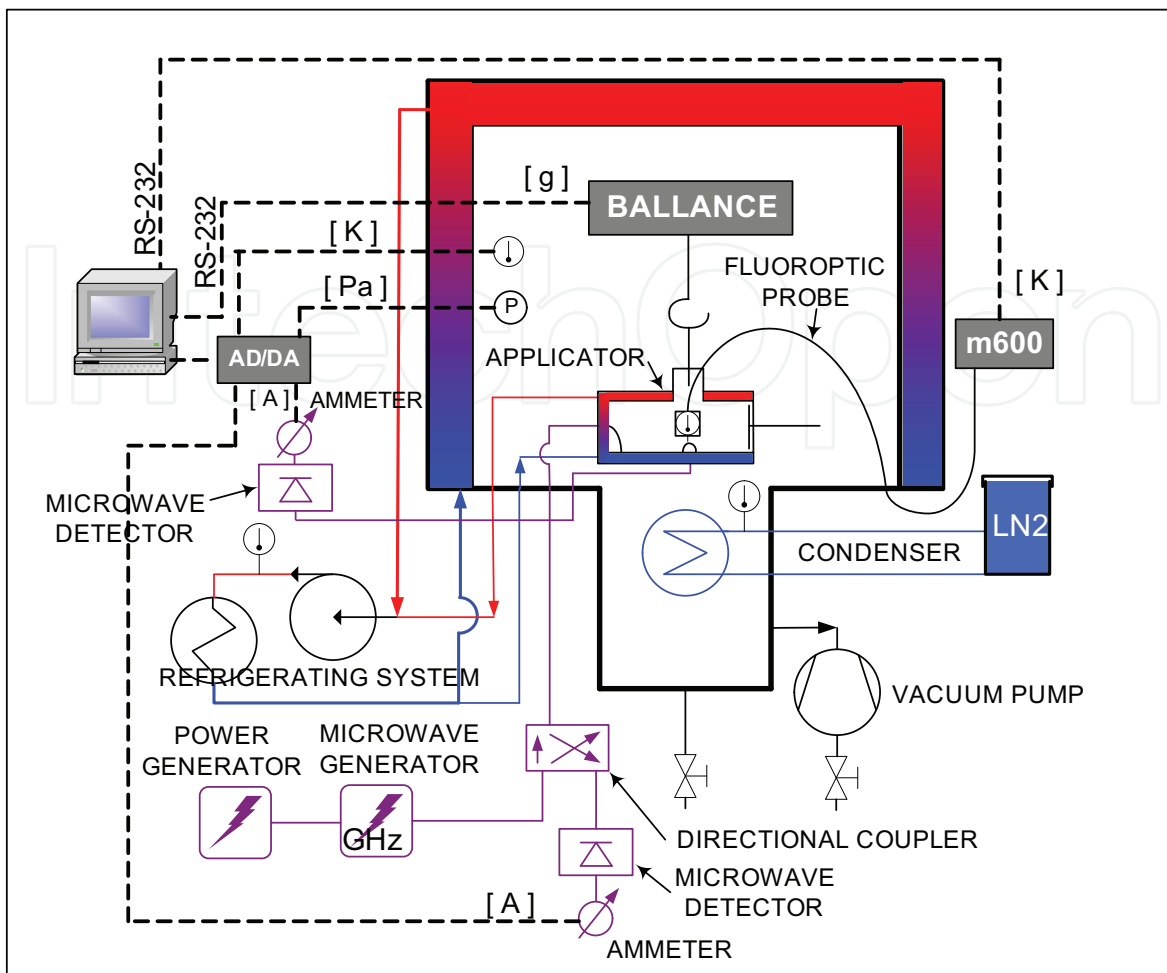


Fig. 1. The experimental set-up for investigations of the primary MFD

Theoretical wavelength in air for this construction amounts to about 15.5 cm, according to the following equation (Metaxas, 1996):

$$\lambda_w = \lambda_0 / \sqrt{1 - \left(\frac{\lambda_0}{2a}\right)^2} \quad (1)$$

where:  $\lambda_0$  - wavelength in air (12.24 cm for frequency  $f=2450$  MHz);  $a$  - height of the waveguide (5 cm). A processed sample should be located at a distance of  $\frac{3}{4}$  wavelength where electric field pattern achieves maximal values.

Tuning of the applicator is performed on the basis of readings of the microwave detector, which is coupled with a magnetic loop under the sample. The current intensity of the detector is directly proportional to electric field strength in the applicator. The applicator is considered to be tuned when current signal of the microwave detector coupled with the magnetic loop under the sample achieves maximum, which means maximal electric field strength in the sample.

## 2.2 Methodology

Experiments of the primary microwave freeze drying were performed in two stages: first with measurements of sample mass decrement and second with only sample temperature

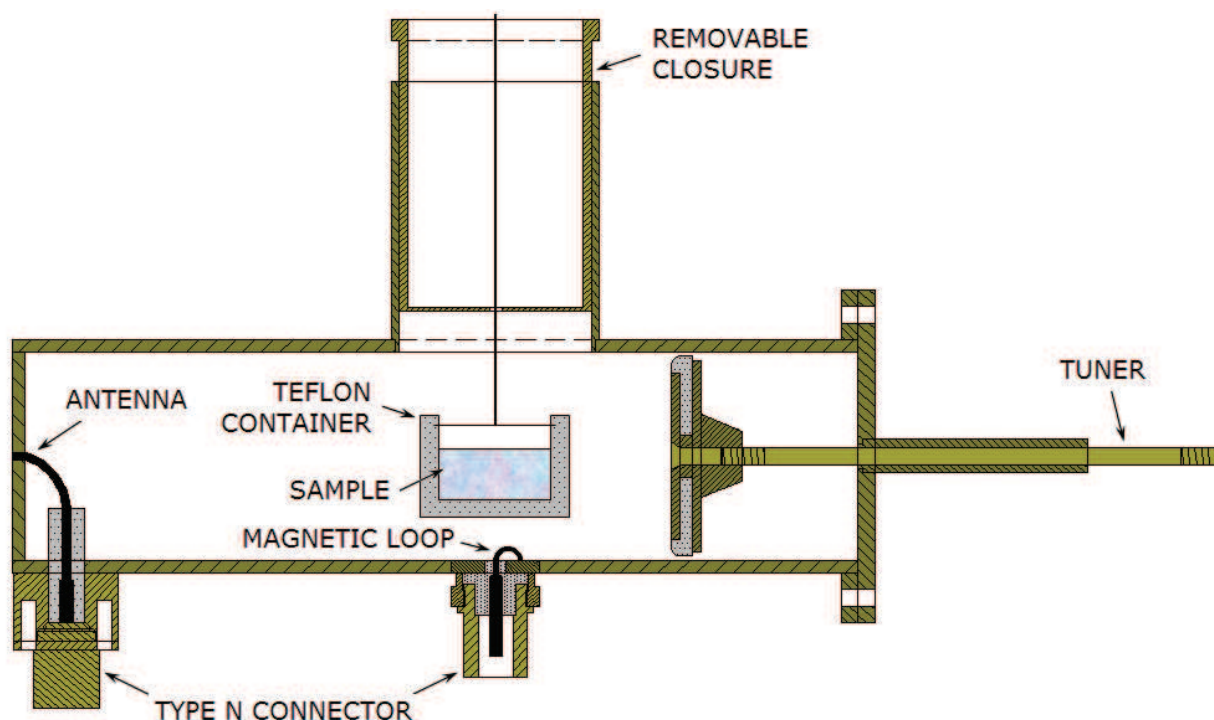


Fig. 2. Cross-section of a waveguide applicator

measurements. It was impossible to measure simultaneously both above mentioned values in the same experimental run. When temperature was measured, a fluoroptic probe was placed in the center of the sample.

After freezing of the wet material in the vacuum chamber at the temperature about  $-50\text{ }^{\circ}\text{C}$ , the apparatus is sealed and the vacuum pump started. When demanded process pressure in the chamber is achieved, the microwave generator is turned on.

When a dried sample is inserted through the removable closure into the applicator, the waveguide is usually shortened and cavity needs to be tuned to a  $\text{TE}_{102}$  mode. However, as dielectric properties of a sample change as a result of moisture content or temperature fluctuations, the cavity length needs to be adjusted accordingly.

During the single experimental run, the sample temperature or sample weight decrement as well as temperature and pressure in the vacuum chamber are recorded by DASyLab data acquisition program. Additionally, continuous measurements of current signal of the microwave detector coupled with magnetic loop inside the applicator indicate when the resonant cavity needs to be tuned during the experiments. Varying during an experimental run current signal may indicate that electric field strength in a dried sample is not constant. These changes were not significant, but taking them into account in mathematical modeling would require derivation of electric field strength distribution in sample layers.

The average power absorbed volumetrically in the dried material (internal heat source capacity) can be calculated provided that  $|E|$  - the magnitude of the electric field strength  $E$  inside the sample is known (Metaxas, 1996; Schiffmann, 2006):

$$Q_v = \frac{1}{2} \omega \epsilon_0 \epsilon' \tan \delta |E|^2 = \pi f \epsilon_0 \epsilon' \tan \delta |E|^2 \quad (2a)$$

or

$$Q_v = \frac{1}{2} \omega \varepsilon_0 \varepsilon'' |E|^2 = \pi f \varepsilon_0 \varepsilon'' |E|^2 \quad (2b)$$

where:  $\tan \delta = \varepsilon''/\varepsilon'$ . In the case of drying of small samples, we can assume uniform electric field inside the material, and then  $|E| = E_0 = \sqrt{2}E_{rms}$ , where  $E_0$  is the peak magnitude of the field and  $E_{rms}$  is the rms value. Applying this simplification to Eq. (2b) gives:

$$Q_v = 2\pi f \varepsilon_0 \varepsilon'' E^2 \quad (3)$$

In this chapter the symbol  $E$  is used instead of  $E_{rms}$  to define the electric field in the material.

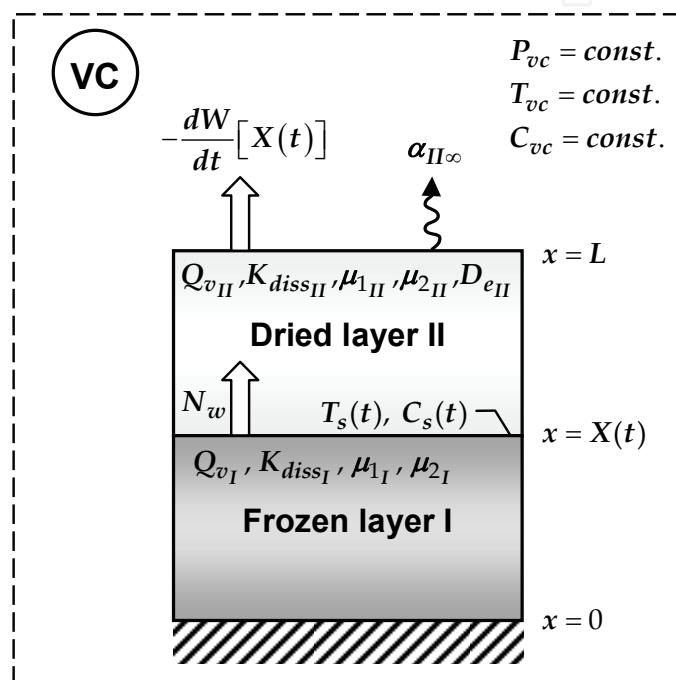


Fig. 3. The physical model of the primary MFD

### 3. Mathematical modeling of the primary MFD

#### 3.1 Model formulation and assumptions

Consider a dried material which has geometry of a slab of infinite length. The sample bottom is insulated for heat and mass transfer and the upper surface is exposed to a vacuum at drying chamber temperature, as shown in Figure 3.

During the primary stage of the process, as sublimated vapors diffuse from the ice front towards exposed surface, moving boundary retreats until frozen free water is totally removed. The ice front (moving boundary) is assumed to be a plane of zero thickness and its initial position is arbitrary defined. In the frozen region *I* energy is transferred by conduction whereas conduction and convection are considered in the dried region *II*.

For dominant polarization of the electric field normal to the sample surface, it can be assumed that the electric field strength is constant throughout the dried material and equal to the value at the surface. Such simplification is justified when the penetration depth of microwaves is much greater than the size of the sample.

### 3.2 Governing equations

The physical system is described by the following differential equations.

*Frozen Region*

Heat transfer:

$$\frac{\partial T_I}{\partial t} = a_{eI} \frac{\partial^2 T_I}{\partial x^2} + \frac{Q_{vI}}{\rho_{buI} c_{pI}} \quad (4)$$

*Dried Region*

Heat transfer:

$$\frac{\partial T_{II}}{\partial t} = a_{eII} \frac{\partial^2 T_{II}}{\partial x^2} - \frac{c_{pw}}{\rho_{buII} c_{pII}} \frac{\partial(N_w T_{II})}{\partial x} + \frac{Q_{vII}}{\rho_{buII} c_{pII}} \quad (5)$$

Steady capacities of internal heat sources in equations (4) and (5) are defined as follows:

$$Q_{v_i} = K_{diss_i}(T_i)E^2 \quad \text{for } i = I, II \quad (6)$$

where dissipation coefficient:

$$K_{diss_i}(T_i) = 2\pi f \varepsilon_0 \varepsilon_i''(T_i) \quad \text{for } i = I, II \quad (7)$$

Here, the dissipation coefficient in above equations is expressed as a linear function of material temperature:

$$K_{diss_i}(T) \approx \mu_1 T + \mu_2 \quad \text{for } i = I, II \quad (8)$$

where parameters  $\mu_1$  and  $\mu_2$  are determined by linear regression of experimental data (Witkiewicz, 2006).

Mass transfer:

$$D_{eII} \frac{\partial^2 C}{\partial x^2} = \frac{\partial C}{\partial t} \quad (9)$$

Effective diffusivity  $D_{eII}$  :

$$\frac{1}{D_{eII}} = \frac{1}{D_K} + \frac{1}{D_M} \quad (10)$$

is a combination of Knudsen diffusivity (Coulson et al., 1999):

$$D_K = 1.0638 \cdot r_p \sqrt{\frac{RT_{II_{avg}}}{M_w}} \quad (11)$$

and molecular diffusivity (Poling et al., 2001):

$$D_M = \frac{1.8829 \cdot T_{II_{avg}}^{3/2} (1/M_w + 1/M_{in})^{1/2}}{P \sigma_{AB}^2 \Omega_{AB}} \quad (12)$$

where  $\sigma_{AB}$  and  $\Omega_{AB}$  are determined for the system water vapor (A) – air (B) on the basis of tabulated constant of Lennard-Jones forces.

#### Sublimation front

The heat flux and mass flux at pseudo-steady-state conditions are related by:

$$q_s = N_w \Delta h_s \quad (13)$$

Then energy balance is:

$$-k_{eI} \frac{\partial T_I}{\partial x} + k_{eII} \frac{\partial T_{II}}{\partial x} = N_w \Delta h_s \quad (14)$$

The displacement of the moving boundary is related to the rate of sublimation:

$$N_w = -(W_{ini} - W_{eq}) \rho_{buII} \frac{dX(t)}{dt} \quad (15)$$

#### Initial Conditions

The initial moving boundary positions can be determined as follows:

$$X(t) = L - \delta, \quad \text{for } t = 0 \quad (16)$$

where arbitrary initial thickness of the dried layer is chosen as  $\delta = 3\%$  of sample thickness. This value of  $\delta$  is used to start the numerical computations of the formulated model. In the frozen layer constant initial temperature is imposed:

$$T_I(x, 0) = T_{ini} \quad \text{for } 0 \leq x \leq X \quad \text{and } t = 0 \quad (17)$$

In the dried layer initial linear temperature and concentration profiles are assumed:

$$\frac{T_L(0) - T_{II}(x, 0)}{T_L(0) - T_{ini}(0)} = \frac{L - x}{\delta} \quad \text{for } X \leq x \leq L \quad \text{and } t = 0 \quad (18)$$

where:

$$T_L(0) = \frac{\alpha_{II\infty}(L-x)T_{vc} + k_{eII}T_s}{\alpha_{II\infty}(L-x) + k_{eII}} \quad \text{for } x = L \quad \text{and } t = 0 \quad (19)$$

$$C = C_{vc} - \left( \frac{\partial C}{\partial x} \right)_{x=X} (L-x) \quad \text{for } X \leq x \leq L \quad \text{and } t = 0 \quad (20)$$

#### Boundary Conditions

There is no heat transfer through the bottom boundary of the material, which is insulated by the wall of a Teflon container:

$$\left( -k_{eI} \frac{\partial T_I}{\partial x} \right)_{x=0} = 0 \quad \text{for } t \geq 0 \quad (21a)$$

There is a heat transfer between the exposed material surface and surroundings:

$$k_{eII} \left( \frac{\partial T_{II}}{\partial x} \right)_{x=L} = \alpha_{II\infty} (T_{vc} - T_L) \quad \text{for } t \geq 0 \quad (21b)$$

At the ice front the thermodynamic equilibrium between water vapor and ice is assumed. Thus the vapor mass concentration at the moving front is related by Clausius-Clapeyron relation:

$$C_s(t) = f(T_s) = \exp\left(\frac{a}{T_s} + b\right) M_w / (RT_s) \quad \text{for } x = X(t) \text{ and } t \geq 0 \quad (21c)$$

where:  $a = -6320.152$  and  $b = 29.558$  (Wolff et al., 1989).

The condenser maintains low pressure of the vacuum chamber, therefore mass transfer resistance at the exposed surface is negligible:

$$C_L(t) = C_{vc} \quad \text{for } x = L \text{ and } t \geq 0 \quad (21d)$$

### 3.3 Methods of model solution

The solution of the one-dimensional moving boundary problem in a planar medium described by Equations (4), (5), (9), (14)-(21) cannot be easily obtained unless some numerical techniques are used. Many approaches have been reported in the literature concerning general moving boundary problem with such phase change as melting, solidification or sublimation. Some researches use a fixed grid, fixed time-step formulation but it fails to give a reliable estimation of the material's temperature near the moving boundary (Yuen & Kleinman, 1980).

Another popular approach is the Landau's transformation (LT) method which mathematically immobilizes the moving boundary so that the number of spatial nodes in the frozen and dried region is constant (Fig. 4b). Such transformed mathematical model can be easily solved using commercial software.

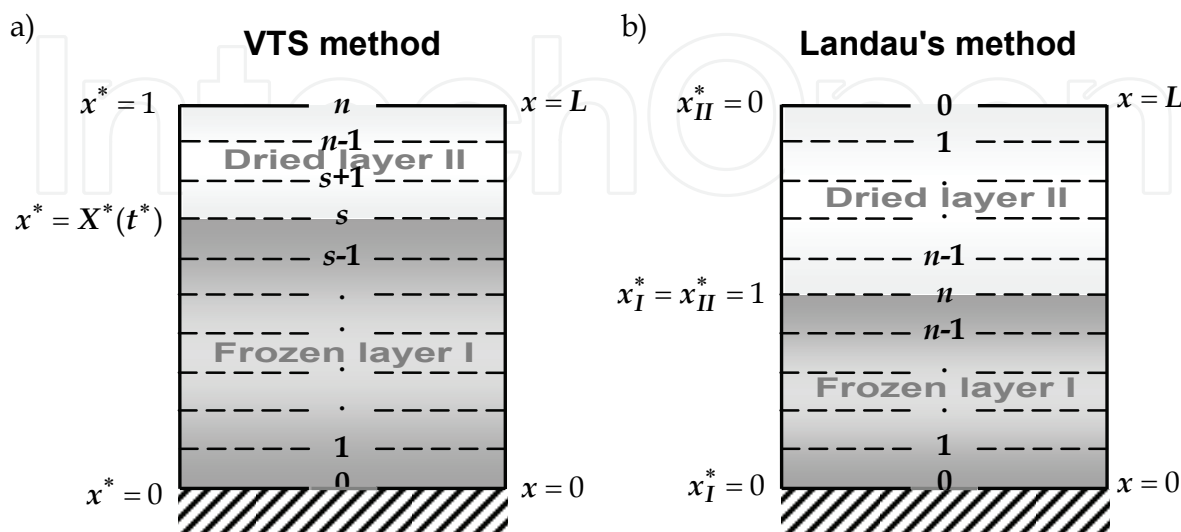


Fig. 4. Discretization grid of spatial variable

In this work, this method is compared with the variable time-step (VTS) approach, introduced as an alternative and effective numerical technique of moving boundary problem solution. The VTS method uses a fixed grid and the time step is adjusted to cause movement of the interface exactly one grid space (Fig. 4a). This approach can be also applied together with the Landau's transformation method.

The formulated mathematical model of the microwave freeze drying was solved numerically using two approaches: VTS and LT.

Equations (4), (5), (9), (14)-(15) make a set of mathematical model equations which are discretized by the implicit finite-difference Crank-Nicolson scheme and solved together with the adequate initial (16)-(20) and boundary conditions (21a)-(21d).

### 3.4 VTS method

The VTS method is a spatial fixed grid approach. The number of spatial nodes in computational grid resulting from discretization is constant. It means that in each step of computations the sublimation ice front should move exactly one grid space from the previous location. Instead of Eqs. (14) and (15) the following simultaneous heat and mass balance at the moving boundary must be fulfilled:

$$-k_{eI} \frac{T_{s,j} - T_{I_{s-1},j}}{\Delta x} - k_{eII} \frac{T_{s,j} - T_{II_{s+1},j}}{\Delta x} - (W_{ini} - W_{eq}) \rho_{buII} \Delta h_s \frac{\Delta x}{\Delta t} - \rho_{buI} c_{pI} \frac{\Delta x}{\Delta t} (T_{s,j} - T_{I_{s,j-1}}) = 0 \quad (22)$$

where in the above finite-difference scheme: the subscript  $s$  represents the space grid location of the ice sublimation interface (moving boundary) and the subscript  $j$  indicates time step.

The individual terms in above equation correspond to heat flux densities transferred from the frozen and dried material regions, heat flux utilized by sublimation and heat required to raise the temperature of interface node from previous time step to current one.

The following dimensionless variables are introduced for the sake of solution convenience:

$$x^* = \frac{x}{L} \quad (23)$$

$$\begin{aligned} X^* &= \frac{X}{L} & t^* &= \frac{a_{eI} t}{L^2} & C^* &= \frac{C - C_{vc}}{C_{s,3} - C_{vc}} \\ T_I^* &= \frac{T_I - T_0}{T_{vc} - T_0} & T_{II}^* &= \frac{T_{II} - T_0}{T_{vc} - T_0} & W^* &= \frac{W - W_{eq}}{W_{ini} - W_{eq}} \end{aligned} \quad (24)$$

where  $W$  denotes the average moisture content of the material bed.

The governing equations (4)-(5), (9) can be now rewritten as:

$$\frac{\partial^2 T_I^*}{\partial x^{*2}} - \frac{\partial T_I^*}{\partial t^*} = - \frac{Q_{V_I} L^2}{k_{eI} (T_{vc} - T_0)} \quad (25)$$

$$\frac{\partial^2 T_{II}^*}{\partial x^{*2}} - \frac{c_{pw} \rho_{buII} a_{eI} (W_{ini} - W_{eq})}{k_{eII}} \frac{dX^*}{dt^*} \frac{\partial T_{II}^*}{\partial x^*} - \frac{a_{eI}}{a_{eII}} \frac{\partial T_{II}^*}{\partial t^*} = - \frac{Q_{V_{II}} L^2}{k_{eII} (T_{vc} - T_0)} \quad (26)$$

$$\frac{\partial^2 C^*}{\partial x^{*2}} - \frac{a_{eI}}{D_{eII}} \frac{\partial C^*}{\partial t^*} = 0 \quad (27)$$

Heat and mass balance at the sublimation front (22) can be rewritten as:

$$-k_{eI} \frac{T_{s,j}^* - T_{I_{s-1,j}}^*}{\Delta x^*} - k_{eII} \frac{T_{s,j}^* - T_{II_{s+1,j}}^*}{\Delta x^*} - \frac{W_{ini} - W_{eq}}{T_{vc} - T_0} \rho_{buII} \Delta h_s a_{eI} \frac{\Delta x^*}{\Delta t^*} - k_{eI} \frac{\Delta x^*}{\Delta t^*} (T_{s,j}^* - T_{I_{s,j-1}}^*) = 0 \quad (28)$$

In each calculation step, value of the actual time step corresponding to one spatial grid space movement is determined iteratively by bisection method as a root of Eq. (28). The initial conditions (16)-(20) become:

$$X^* = \frac{\delta}{L} \quad \text{for} \quad t^* = 0 \quad (29a)$$

$$T_I^* = 0 \quad \text{for} \quad 0 \leq x^* < X^* \quad \text{and} \quad t^* = 0 \quad (29b)$$

$$T_{II}^* = \left(1 - \frac{1 - x^*}{1 - X^*}\right) T_{II_L}^* \quad \text{for} \quad X^* \leq x^* \leq 1 \quad \text{and} \quad t^* = 0 \quad (29c)$$

$$C^* = \frac{k_{eII} (T_{vc} - T_{ini}) T_{II_L}^*}{D_{eII} (C_{s,3} - C_{vc}) \Delta h_s} x_{II}^* \quad \text{for} \quad X^* \leq x^* \leq 1 \quad \text{and} \quad t^* = 0 \quad (29d)$$

where

$$T_{II_L}^* = \frac{\alpha_{II\infty} L (1 - X^*)}{\alpha_{II\infty} L (1 - X^*) + k_{eII}} \quad \text{for} \quad x^* = 1 \quad \text{and} \quad t^* = 0 \quad (29e)$$

The boundary conditions (21a)-(21d) become:

$$\frac{\partial T_I^*}{\partial x^*} = 0 \quad \text{for} \quad x^* = 0 \quad \text{and} \quad t^* > 0 \quad (30a)$$

$$T_{II}^* - \frac{k_{eII}}{\alpha_{II\infty} L} \frac{\partial T_{II}^*}{\partial x^*} - 1 = 0 \quad \text{for} \quad x^* = 1 \quad \text{and} \quad t^* > 0 \quad (30b)$$

$$C^* = f(T_{II}^*) \quad \text{for} \quad x^* = X^* \quad \text{and} \quad t^* > 0 \quad (30c)$$

$$C^* = 0 \quad \text{for} \quad x^* = 0 \quad \text{and} \quad t^* > 0 \quad (30d)$$

Finite difference schemes of Eqs. (25)-(28) together with the initial (29a)-(29e) and boundary conditions (30a)-(30d) constitute the algebraic linear equations set, and can be easily solved by the tridiagonal algorithm. The actual moving boundary position  $X_j^*$  versus time was computed as:  $X_j^* = X_0^* - \Delta x^* \cdot j$ , where  $j$  means the actual number of time steps.

Analogically, the actual average moisture content  $W_j^*$  versus time was computed as:  $W_j^* = W_0^* - \Delta W^* \cdot j$ , where  $\Delta W^* = \Delta x^*$ .

### 3.5 LT method

The Landau's transformation converts the problem of a moving boundary to that of a fixed boundary (Ma & Peltre, 1973) by introducing the following definitions of dimensionless position coordinates in the frozen and dried region:

$$x_I^* = \frac{x}{X(t)} \quad (31a)$$

$$x_{II}^* = \frac{L-x}{L-X(t)} \quad (31b)$$

They are used in conjunction with the dimensionless variables (24) defined in the same way as in the VTS model. The mathematical model equations (4), (5), (9), (14)-(15) have now more complex dimensionless form.

Heat transfer in the frozen layer is:

$$\frac{\partial^2 T_I^*}{\partial x_I^{*2}} + x_I^* X^* \frac{dX^*}{dt^*} \frac{\partial T_I^*}{\partial x_I^*} - X^{*2} \frac{\partial T_I^*}{\partial t^*} = -\frac{Q_{V_I} L^2}{k_{e_I} (T_{vc} - T_0)} X^{*2} \quad (32)$$

Heat and mass transfer in the dried layer are as follows:

$$\begin{aligned} \frac{\partial^2 T_{II}^*}{\partial x_{II}^{*2}} - \left[ \frac{c_{pw} \rho_{bu_{II}} a_{e_I} (W_{ini} - W_{eq})}{k_{e_{II}}} + \frac{a_{e_I} x_{II}^*}{a_{e_{II}}} \right] (1-X^*) \frac{dX^*}{dt^*} \frac{\partial T_{II}^*}{\partial x_{II}^*} + \\ - \frac{a_{e_I} (1-X^*)^2}{a_{e_{II}}} \frac{\partial T_{II}^*}{\partial t^*} = -\frac{Q_{V_{II}} L^2}{k_{e_{II}} (T_{vc} - T_{ini})} (1-X^*)^2 \end{aligned} \quad (33)$$

$$\frac{\partial^2 C^*}{\partial x_{II}^{*2}} - \frac{a_{e_I} x_{II}^* (1-X^*)}{D_{e_{II}}} \frac{dX^*}{dt^*} \frac{\partial C^*}{\partial x_{II}^*} - \frac{a_{e_I} (1-X^*)^2}{D_{e_{II}}} \frac{\partial C^*}{\partial t^*} = 0 \quad (34)$$

Heat and mass balance at the sublimation front:

$$-\frac{T_{vc} - T_{ini}}{L} \left[ \frac{k_{e_{II}}}{(1-X^*)} \left( \frac{\partial T_{II}^*}{\partial x_{II}^*} \right)_{x_{II}^*=1} + \frac{k_{e_I}}{X^*} \left( \frac{\partial T_I^*}{\partial x_I^*} \right)_{x_I^*=1} \right] = N_w \Delta h_s \quad (35)$$

Displacement of the interface:

$$N_w = \frac{D_{e_{II}} (C_{s,3} - C_{vc})}{L(1-X^*)} \left( \frac{\partial C^*}{\partial x_{II}^*} \right)_{x_{II}^*=1} = -\frac{\rho_{bu_{II}} a_{e_I} (W_{ini} - W_{eq})}{L} \frac{dX^*}{dt^*} \quad \text{for } t^* \geq 0 \quad (36)$$

The initial conditions (16)-(20) become:

$$X^* = \frac{\delta}{L} \quad \text{for} \quad x_I^* = x_{II}^* = 1 \quad \text{and} \quad t^* = 0 \quad (37a)$$

$$T_I^* = 0 \quad \text{for} \quad 0 \leq x_I^* \leq 1 \quad \text{and} \quad t^* = 0 \quad (37b)$$

$$T_{II}^* = (1 - x_{II}^*) T_L^* \quad \text{for} \quad 0 \leq x_{II}^* \leq 1 \quad \text{and} \quad t^* = 0 \quad (37c)$$

$$C^* = \frac{k_{eII} (T_{vc} - T_0) T_L^*}{D_{eII} (C_{s,3} - C_{vc}) \Delta h_s} x_{II}^* \quad \text{for} \quad 0 \leq x_{II}^* \leq 1 \quad \text{and} \quad t^* = 0 \quad (37d)$$

where

$$T_L^* = \frac{\alpha_{II\infty} L (1 - X^*)}{\alpha_{II\infty} L (1 - X^*) + k_{eII}} \quad \text{for} \quad x_{II}^* = 0 \quad \text{and} \quad t^* = 0 \quad (37e)$$

The boundary conditions (21a)-(21d) become:

$$\frac{\partial T_I^*}{\partial x_I^*} = 0 \quad \text{for} \quad x_I^* = 0 \quad \text{and} \quad t^* \geq 0 \quad (38a)$$

$$T_{II}^* - \frac{k_{eII}}{\alpha_{II\infty} (1 - X^*)} \frac{\partial T_{II}^*}{\partial x_{II}^*} - 1 = 0 \quad \text{for} \quad x_{II}^* = 0 \quad \text{and} \quad t^* \geq 0 \quad (38b)$$

$$C^* = f(T_s^*) \quad \text{for} \quad x_I^* = x_{II}^* = 1 \quad \text{and} \quad t^* \geq 0 \quad (38c)$$

$$C^* = 0 \quad \text{for} \quad x_{II}^* = 0 \quad \text{and} \quad t^* \geq 0 \quad (38d)$$

Finite difference schemes of Eqs. (32)-(36) together with the initial (37a)-(37e) and boundary conditions (38a)-(38d) constitute the algebraic nonlinear equations set, and it must be solved by the adequate numerical algorithm.

Both the frozen and dried layer was divided into 20 equal space intervals. Resulting algebraic nonlinear equations set was solved in each time step by means of adequate numerical procedure in the Mathcad software.

In the LT method the actual moving boundary position  $X^*$  versus time was computed from solution of the set of discretized governing equations (32)-(36). The actual average moisture content of the drying bed  $W_j^*$  versus time was computed as:  $W_j^* = W_0^* - \Delta W^* \cdot j$ , where  $\Delta W^* = \Delta x^*$ .

### 3.6 Modeling results of the MFD primary stage

The simulations of the MFD were performed using two described above numerical methods for three selected materials: Sorbonorit 4, beef and mannitol. Thermophysical properties and parameters of the Sorbonorit 4 MFD system are presented in Table 1. The thermophysical parameters of the beef were taken from paper (Ma & Peltre, 1973, 1975a, b). While the analogical data for mannitol is included in the article (Wang & Chen, 2003). The exemplary simulations results of the MFD of selected materials using the VTS and LT approach are shown in Figs. 5 through 7.

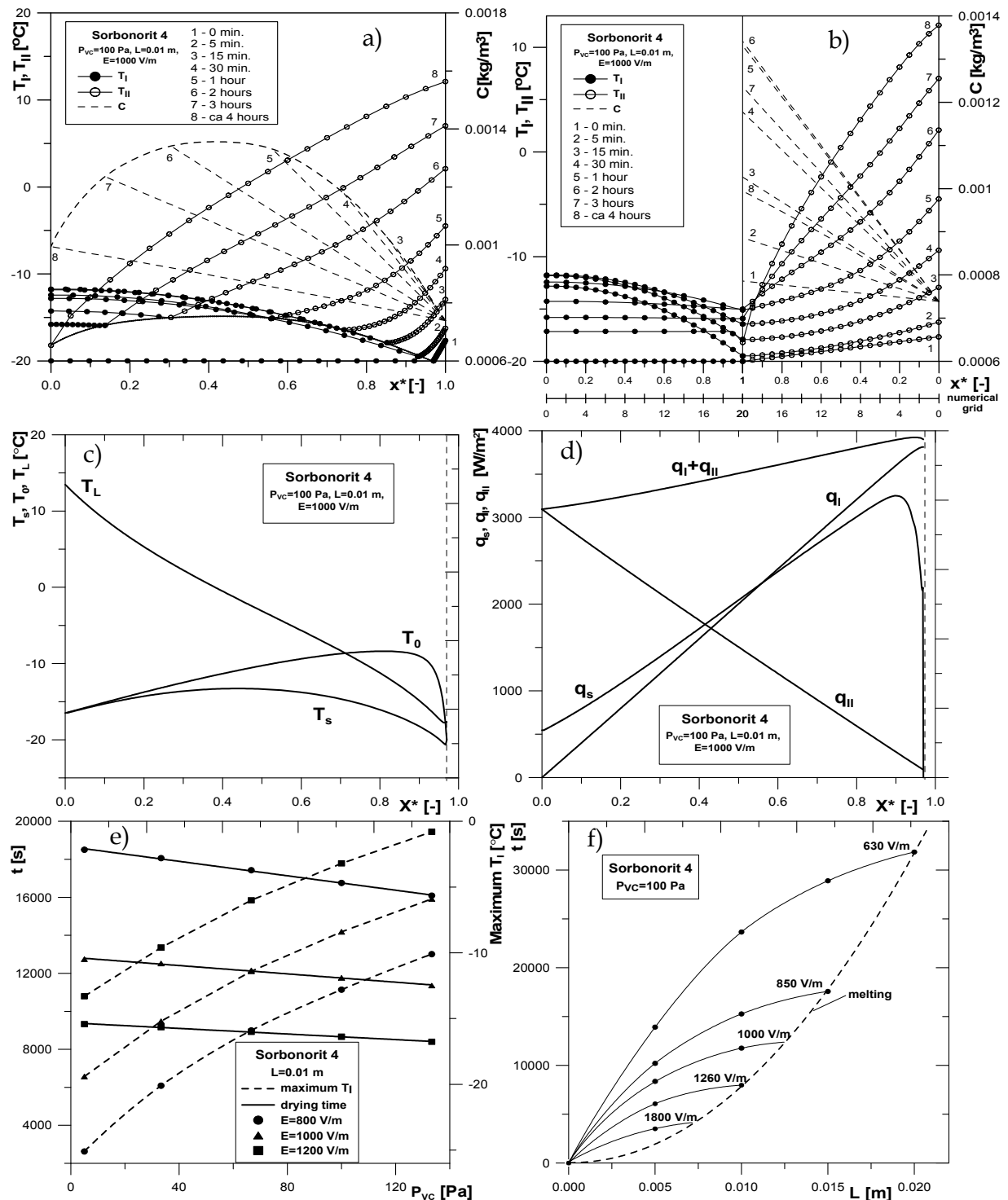


Fig. 5. Exemplary simulation results of Sorbonorit MFD: a) temperature and vapor concentration profiles for various process times – VTS method and b) LT method; c) temperature evolution on the sample surface  $T_L$ , sample bottom  $T_0$  and sublimation front  $T_s$  versus dimensionless MB position; d) heat flux densities generated in the frozen layer  $q_I$ , in dried layer  $q_{II}$  and at MB  $q_s$  versus dimensionless MB position; e) effects of the total pressure on the drying time and maximum temperature of the frozen region; f) effects of the sample thickness on the total drying time for various electric field strengths.

Material thickness $L$	0.005÷0.02 m	Initial thickness $\delta$	0.03 · $L$ m
Elec. field strength $E$	630÷1800 V/m	VC pressure $P_{vc}$	5÷133.33 Pa
Ambient temp. $T_{vc}$	20 °C	Initial temperature $T_{ini}$	-20 °C
Heat trans. coeff. $\alpha_{II\infty}$	20 W/(m <sup>2</sup> K)	Bed porosity $\varepsilon$	0.71 m <sup>3</sup> /m <sup>3</sup>
Avg. moist. cont. $W_{eq}$	0.05 kg/kg	Eq. moisture content $W_{ini}$	1.63 kg/kg
Layer parameter	Frozen layer i=I	Dried layer i=II	
Thermal diffusivity $a_{e_i}$	1.54 m <sup>2</sup> /s (100 Pa)	0.30 m <sup>2</sup> /s (100 Pa)	
Thermal conductivity $k_{e_i}$	1.60 W/mK (100 Pa)	0.094 W/mK (100 Pa)	
Parameter in Eq. (8) $\mu_{1_i}$	0.00090 W/(KmV <sup>2</sup> )	0.00079 W/(KmV <sup>2</sup> )	
Parameter in Eq. (8) $\mu_{2_i}$	0.41148 W/(mV <sup>2</sup> )	0.30905 W/(mV <sup>2</sup> )	
Density $\rho_{e_i}$	1048 kg/m <sup>3</sup>	400 kg/m <sup>3</sup>	

Table 1. Thermophysical properties and parameters of the Sorbonorit 4 MFD system

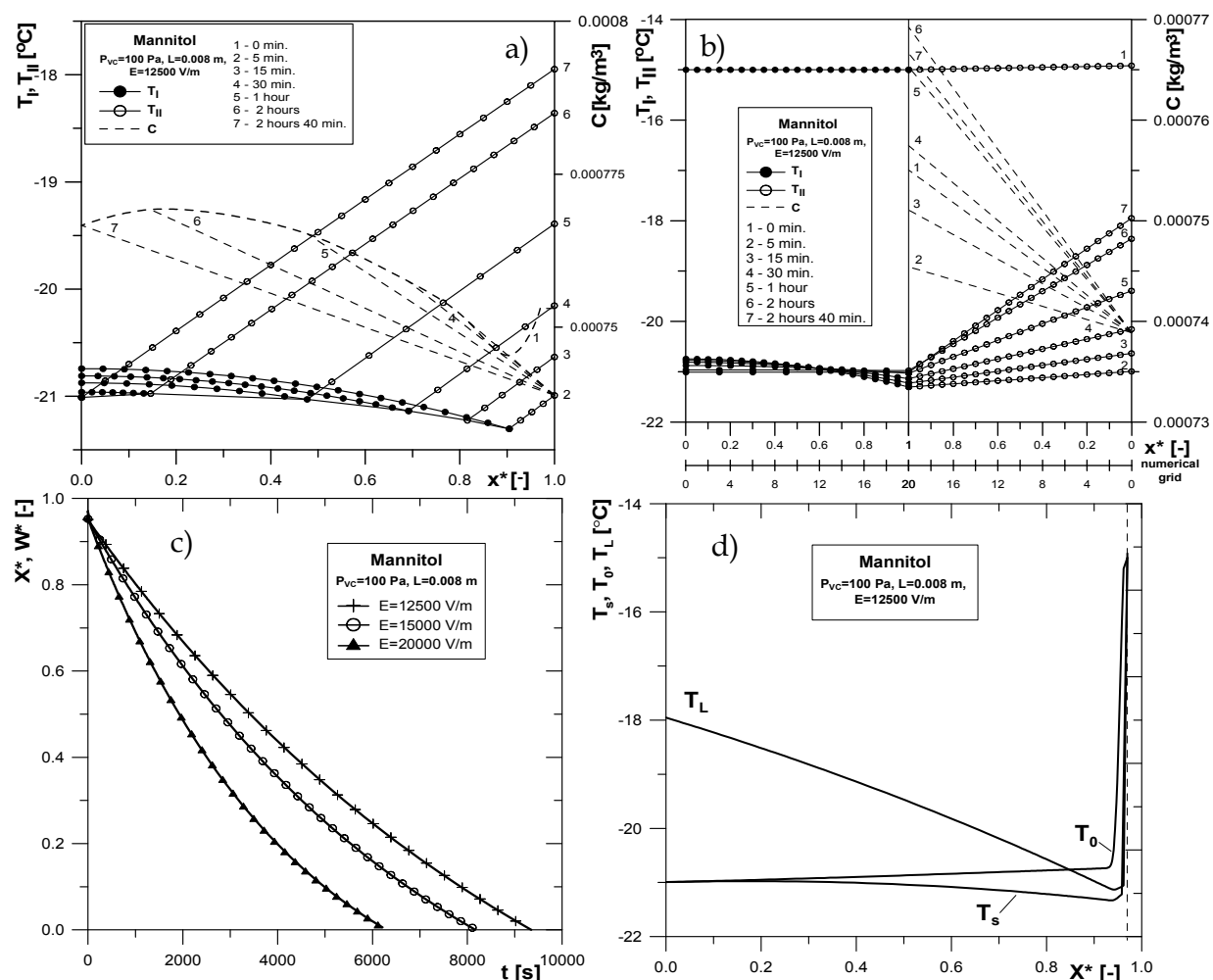


Fig. 6. Exemplary simulation results of mannitol MFD: a) temperature and vapor concentration profiles in the sample for various process times – VTS method and b) LT method; c) drying curves; d) temperature evolution on the sample surface  $T_L$ , sample bottom  $T_0$  and sublimation front  $T_s$  versus dimensionless MB position.

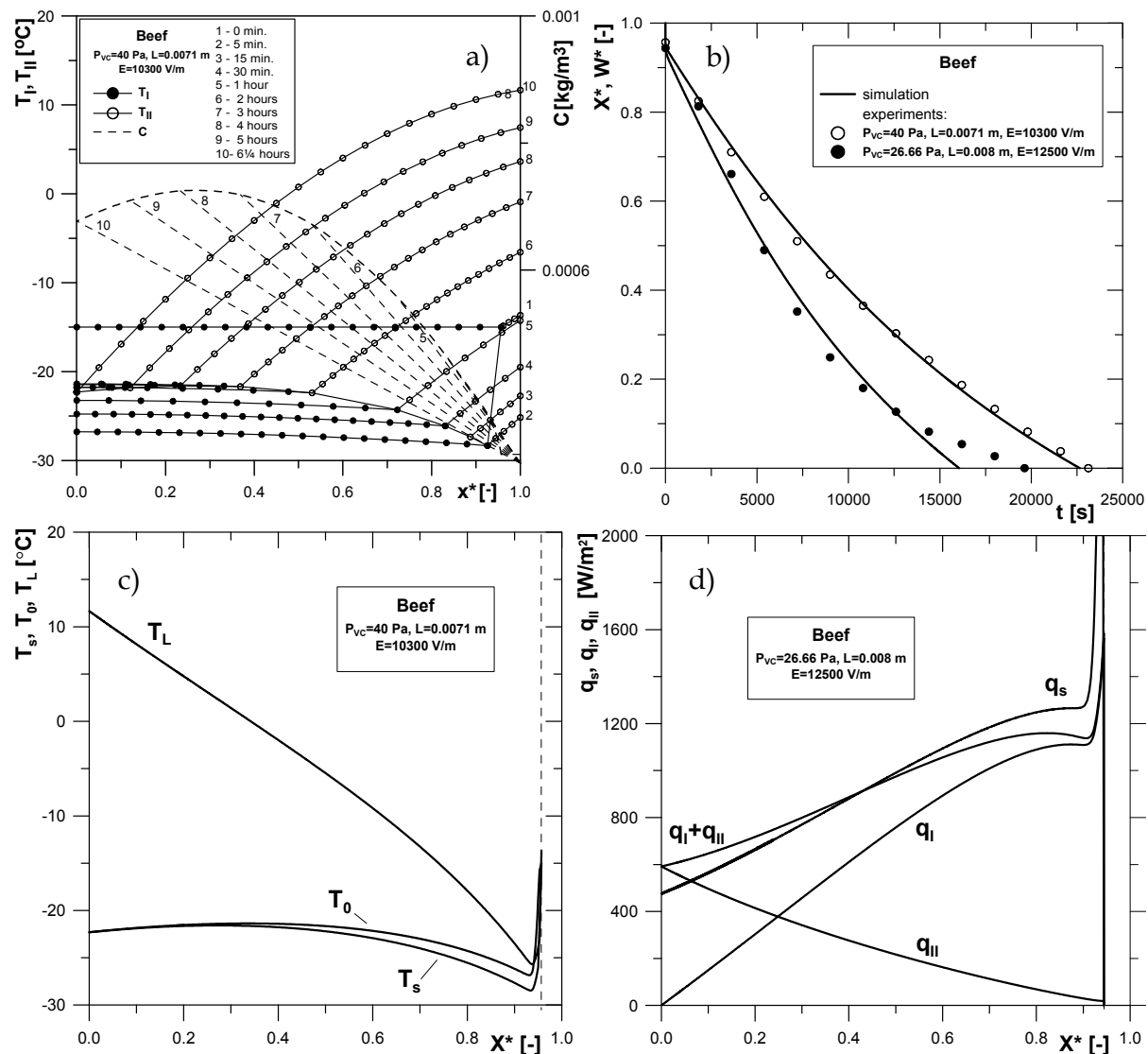


Fig. 7. Exemplary simulation and experimental results of beef MFD: a) temperature and vapor concentration profiles in the sample for various process times – VTS method and b) drying curve; c) temperature evolution on the sample surface  $T_L$ , sample bottom  $T_0$  and sublimation front  $T_s$  versus dimensionless MB position; d) heat flux densities generated in the frozen layer  $q_I$ , in dried layer  $q_{II}$  and at the MB  $q_s$  versus dimensionless MB position.

The heat flux densities:  $q_I$  and  $q_{II}$  presented in the Figs. 5 through 7 were computed in the actual time step as follows:  $q_i = \sum Q_{v_{i,j}} \Delta x$ , for  $i=1,2$ , where  $j$  denotes number of the node in the difference scheme. The heat flux density at the sublimation front  $q_s$  was determined from the Eqs. (14) and (15) for the actual time step  $\Delta t$  and MB movement  $\Delta X$ .

The objective of these simulations is to determine the optimal control policy of the MFD primary stage of the selected materials to improve drying rate and simultaneously achieve desired product quality. The vacuum chamber pressure  $P_{vc}$  and microwave power  $E$  are considered the controllable factors in the MFD system in order to avoid gas breakdown (corona discharge) and melting. The corona discharge occurs when the electric field intensity is above the threshold value. The ionization of the residual gases in the vacuum

chamber leads to great energy losses and can seriously damage the final product. Since the electric field intensity  $E$  is proportional to the power applied by the microwave generator, its settings should be controlled during the process. The threshold value of the electric field is a function of chamber pressure and has the minimum in the typical pressure range used in freeze-drying (10 – 300 Pa). Therefore upper limit on the electric field strength should be set. Another limits need to be set on the temperature maxima in the dried product to keep its demanded quality. The temperature throughout the dried layer must be lower than the melting temperature and the temperature throughout the dried layer must not exceed the scorch temperature. The melting temperature of frozen foodstuffs is lower than the melting temperature of pure ice, due to existence of soluble chemical compounds in the material. This value amounts usually to  $-3 \div -1.5^\circ\text{C}$  for foodstuffs (Ma & Peltre, 1975; Ang et al., 1977). The scorch temperature of the dried layer is a temperature of material thermal degradation and typically amounts to  $50 \div 60^\circ\text{C}$ . More restrictive temperature constraints are set in microwave freeze-drying of biological and pharmaceutical products, when biological activity is an important quality factor.

In Figure 5e the drying time and maximal temperatures reached in the frozen region are plotted as a function of the vacuum chamber pressure at various electric field strengths for Sorbonorit 4 bed ( $L=0.01\text{ m}$ ). As can be seen, the drying time varies strongly with the electric field strength and is generally linearly depended on  $1/E^2$ . Increase of the vacuum chamber pressure decreases the drying time. It is caused by improved heat transfer in dried layer. Simultaneously, the temperatures in the material increase as a result of the greater diffusion mass transfer resistances in the dried layer. As dissipation coefficients are linearly temperature dependent, the internal heat source capacity is greater and implies intensification of the process. The maximal temperatures reached in the frozen region, shown in Figure 5e, indicate that increasing the vacuum chamber pressure and electric field strength has its limit and exceeding some constraints causes melting. The influence of the sample thickness on the drying time at various electric field strengths is shown in Figure 5f. Analysis of this relation leads to conclusion that smaller sample thickness would enable using higher electric field strengths. It should significantly shorten the drying time providing that all set constraints are not violated.

## 4. Mathematical modeling of the secondary MFD

### 4.1 Model formulation and assumptions

After primary drying, residual moisture content may be as high as 7% (Rowe & Snowman, 1978). Secondary drying is intended to reduce this to an optimum value for material stability – usually with moisture content between 0.5 and 2.0 %. In secondary stage of the MFD there is not any ice and bound water in the material bed (by means of surface forces) is removed by desorption (Fig. 8).

In formulating of the mathematical model of the secondary MFD the following assumptions are made:

- Initial average moisture content of material is equal to the equilibrium moisture content at average temperature of dried layer at the end of the primary freeze drying.
- Distribution of electric field in a sample is assumed to be uniform. Dissipation coefficient value in the whole material bed corresponds with that of dried region  $K_{dissII}$  in the primary freeze drying stage.

- There are two mechanisms of mass transport in the material: moisture desorption and diffusion of water vapor throughout the bed.
- Gas phase in dried material and in vacuum chamber consists of water vapor and air (inert).
- Adsorption equilibrium is described by multitemperature Langmuir isotherm.

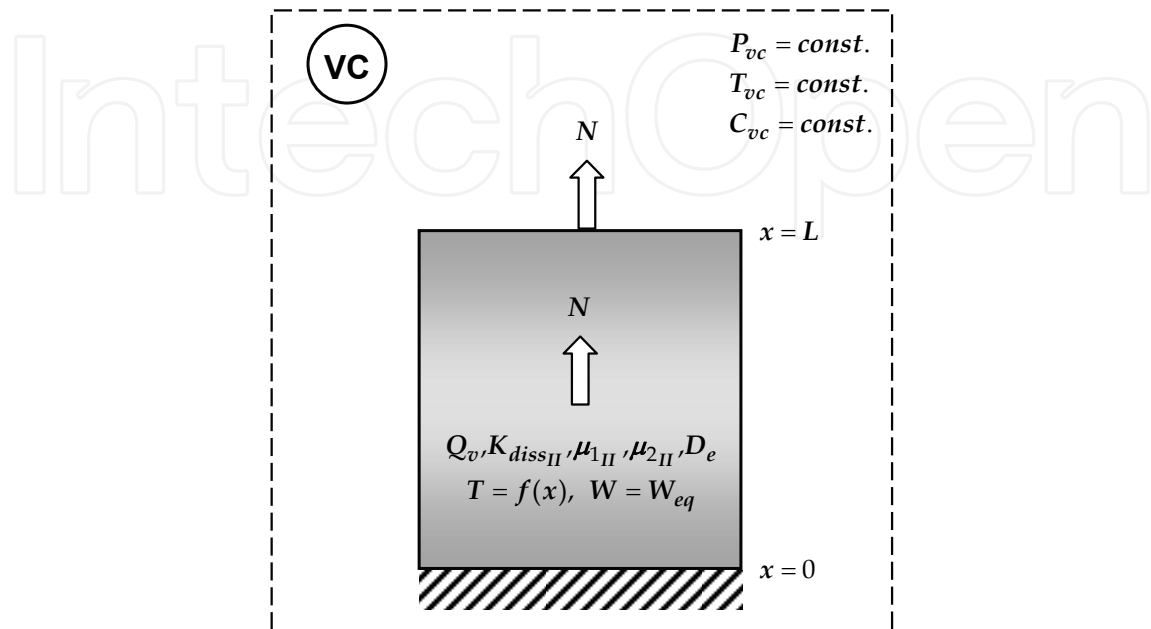


Fig. 8. The physical model of the secondary MFD

#### 4.2 Governing equations

Mass conservation:

$$\frac{\partial(y_w \cdot C)}{\partial t} + \frac{\partial(y_w \cdot N)}{\partial x} + \frac{\rho_{buII}}{\varepsilon \cdot M_w} \frac{\partial W}{\partial t} = 0 \quad (39)$$

where  $y_w + y_{in} = 1$  and  $C = P / RT$  is a sum of molar concentrations of components in gas phase including inert (air).

Moisture mass balance in solid phase results from driving force between equilibrium moisture content and actual moisture content of a material:

$$\frac{\partial W}{\partial t} = K(W_{eq} - W) \quad (40)$$

Adsorption equilibrium is expressed by multitemperature extended Langmuir isotherm (Chahbani & Tondeur, 2001):

$$W_{eq} = W_L \exp\left(\frac{a}{T}\right) \left[ \frac{b \cdot \exp\left(\frac{c}{T}\right) P \cdot y_w}{1 + b \cdot \exp\left(\frac{c}{T}\right) P \cdot y_w} \right] \quad (41)$$

where  $W_L$ ,  $a$ ,  $b$  and  $c$  are the Langmuir equation constants.

Mass transfer:

Kinetic coefficient  $K$  in Equation (40) is calculated applying the linear driving force conception (LDF) (Glueckauf, 1955):

$$K = \frac{60 \cdot D_{eff}}{d_e^2} \quad (42)$$

The mechanism determining vacuum desorption process is the diffusion rate in material pores which is a combination of Knudsen and surface diffusion. Thus, effective diffusivity can be expressed as:

$$D_{eff} = D_S + D_K \frac{\varepsilon_p M_w}{\rho_p} \frac{\partial y_{w,eq}}{\partial W} \quad (43)$$

where  $\varepsilon_p$  and  $\rho_p$  denote particle porosity and particle density, respectively.

Heat transfer:

Quasi-homogeneous heat balance equation can be expressed as:

$$-k_{eII} \frac{\partial^2 T}{\partial x^2} + N \sum_{i=1}^2 y_i c_{pgi} \frac{\partial T}{\partial x} + c_\Sigma \frac{\partial T}{\partial t} + \Delta H_{ads} \frac{\rho_{buII}}{M_w} \frac{\partial W}{\partial t} - Q_v = 0 \quad (44)$$

where  $c_\Sigma$  denotes total volumetric specific heat defined as::

$$c_\Sigma = \rho_{buII} (c_s + Wc_w) + \varepsilon \cdot C \sum_{i=1}^2 y_i c_{pgi} \quad (45)$$

Values  $c_w$  and  $c_s$  are the specific heat capacities of liquid water and dry material sample, respectively.

Isosteric adsorption heat of water vapor in dried material included in Equation (41) is estimated from Clausius-Clapeyron type equation (Do, 1998):

$$\Delta H_{ads} = -RT^2 \left( \frac{\partial \ln P}{\partial T} \right)_W \quad (46)$$

Above equation after incorporating multitemperature Langmuir isotherm can be rewritten in analytical form:

$$\Delta H_{ads} = - \frac{R \cdot W_L \exp(a/T)}{W_L \exp(a/T) - W} \left( a + c - \frac{W \cdot c}{W_L \exp(a/T)} \right) \quad (47)$$

Source term in Equation (44) resulting from dissipation of microwave energy in material volume is defined as:

$$Q_v = K_{dissII} E^2 \quad (48)$$

Dissipation coefficient  $K_{dissII}$  in Equation (48) is expressed as a linear function of material temperature (similarly as in equation (8)):

$$K_{dissII}(T) \approx \mu_{1II}T + \mu_{2II} \quad (49)$$

where parameters  $\mu_1$  and  $\mu_2$  are determined by linear regression of experimental data (Witkiewicz, 2006).

*Momentum balance*

Pressure drop along the sample axis is described by Ergun relation (Ergun, 1952):

$$\frac{\partial P}{\partial x} = -\frac{\eta}{C \cdot k_D} N - \sum_{i=1}^2 y_i M_i \frac{k_E}{C k_D} N^2 \quad (50)$$

where  $i=1$  denotes water vapor and  $i=2$  means inert gas (air).

Parameter  $k_D$  in above Equation defines permeability of dried bed and  $k_E$  parameter describes inertial effect:

$$k_D = \frac{d_e^2 \varepsilon^3}{150(1-\varepsilon)^2}; \quad k_E = \frac{1.75 d_e}{150(1-\varepsilon)} \quad (51)$$

In order to simplify calculation the following relation defining molar flux density of water vapor is derived (Sun et. al, 1995):

$$N = -\frac{2Ck_D\eta^{-1}\partial P/\partial x}{1 + \sqrt{1 + 4C \cdot \left(\sum_{i=1}^2 y_i M_i\right) k_D k_E \eta^{-2} |\partial P/\partial x|}} \quad (52)$$

*Boundary and initial conditions*

Formulated mathematical model is solved together with the following boundary and initial conditions:

$$\frac{\partial y_i}{\partial x} = 0; \quad \frac{\partial P}{\partial x} = 0; \quad \frac{\partial T}{\partial x} = 0 \quad \text{for } x=0 \quad (53a)$$

$$\frac{\partial T}{\partial x} = 0; \quad P = P(t) \quad \text{for } x=L \quad (53b)$$

$$W = W(x,0); \quad T = T(x,0); \quad P = P(x,0) \quad \text{for } t=0 \quad (54)$$

### 4.3 Solution of the mathematical model

*Dimensionless variables*

Model equations can be expressed in more convenient dimensionless form incorporating the following definitions of dimensionless variables:

$$\begin{aligned} t^* &= \frac{a_{eII} t}{L^2}; \quad x^* = \frac{x}{L}; \quad P^* = \frac{P}{\Delta P}; \quad T^* = \frac{T - T_0}{\Delta T} \\ W^* &= \frac{W - W_{eq}}{W_{ini} - W_{eq}}; \quad C_w^* = \frac{y_w C}{C_{w0}}; \quad Q_v^* = Q_v L^2 / (k_e \Delta T); \end{aligned} \quad (55)$$

where pressure and temperature are normalized relatively to arbitrary chosen increments  $\Delta P$  and  $\Delta T$  respectively.

Governing equations in dimensionless form

Mathematical model after transformation consists of mass balance in gas phase:

$$a_{eII} C_{w0} \frac{\partial C_w^*}{\partial t^*} + L \frac{\partial (y_w \cdot N)}{\partial x^*} + \frac{a_{eII} \rho_{buII} (W_{ini} - W_{eq})}{\varepsilon M_w} \frac{\partial W^*}{\partial t^*} = 0 \quad (56)$$

mass balance in solid phase:

$$\frac{\partial W^*}{\partial t^*} = - \frac{L^2}{a_{eII}} K W^* \quad (57)$$

quasi-homogeneous heat balance:

$$-k_{eII} \frac{\partial^2 T^*}{\partial x^{*2}} + LN \sum_{i=1}^2 y_i c_{pgi} \frac{\partial T^*}{\partial x^*} + LC_{\Sigma} \frac{\partial T^*}{\partial t^*} + \frac{a_{eII} (W_{ini} - W_{eq}) \rho_{buII} \Delta H_{ads}}{\Delta T M_w} \frac{\partial W^*}{\partial t^*} - k_{eII} Q_v^* = 0 \quad (58)$$

and Ergun equation:

$$\Delta P \frac{\partial (P^*)}{\partial x^*} = - \frac{L \eta}{C k_D} N - \left( \sum_{i=1}^2 y_i M_i \right) \frac{L k_E}{C k_D} N^2 \quad (59)$$

where  $W^*$  is expressed by multitemperature extended Langmuir isotherm.

Mathematical model is solved numerically by means of numerical method of lines (NMOL) which requires transformation of partial differential equations into set of ordinary differential equations for time derivatives, and approximation of space derivatives by adequate finite differences (Schiesser, 1991).

#### 4.4 Modeling results of the MFD secondary stage

In theoretical analysis the vacuum desorption of water in Zeolite DAY-20F at microwave heating is considered. Parameters of multitemperature Langmuir isotherm (Eq. (41)) for water-Zeolite DAY-20F system listed in Table 2 were approximated by nonlinear Levenberg-Marquardt estimation of data within temperature range of 293÷373 K (Sun et al., 1995).

Component	Constants of multitemperature Langmuir isotherm equation			
	$W_L$ , kg /kg	$a$ , K	$b$ , Pa <sup>-1</sup>	$c$ , K
Water	0.370300	1387.82	0.170 · 10 <sup>-6</sup>	1511.02

Table 2. Constants of multitemperature Langmuir isotherm equation for water-Zeolite DAY- 20F system

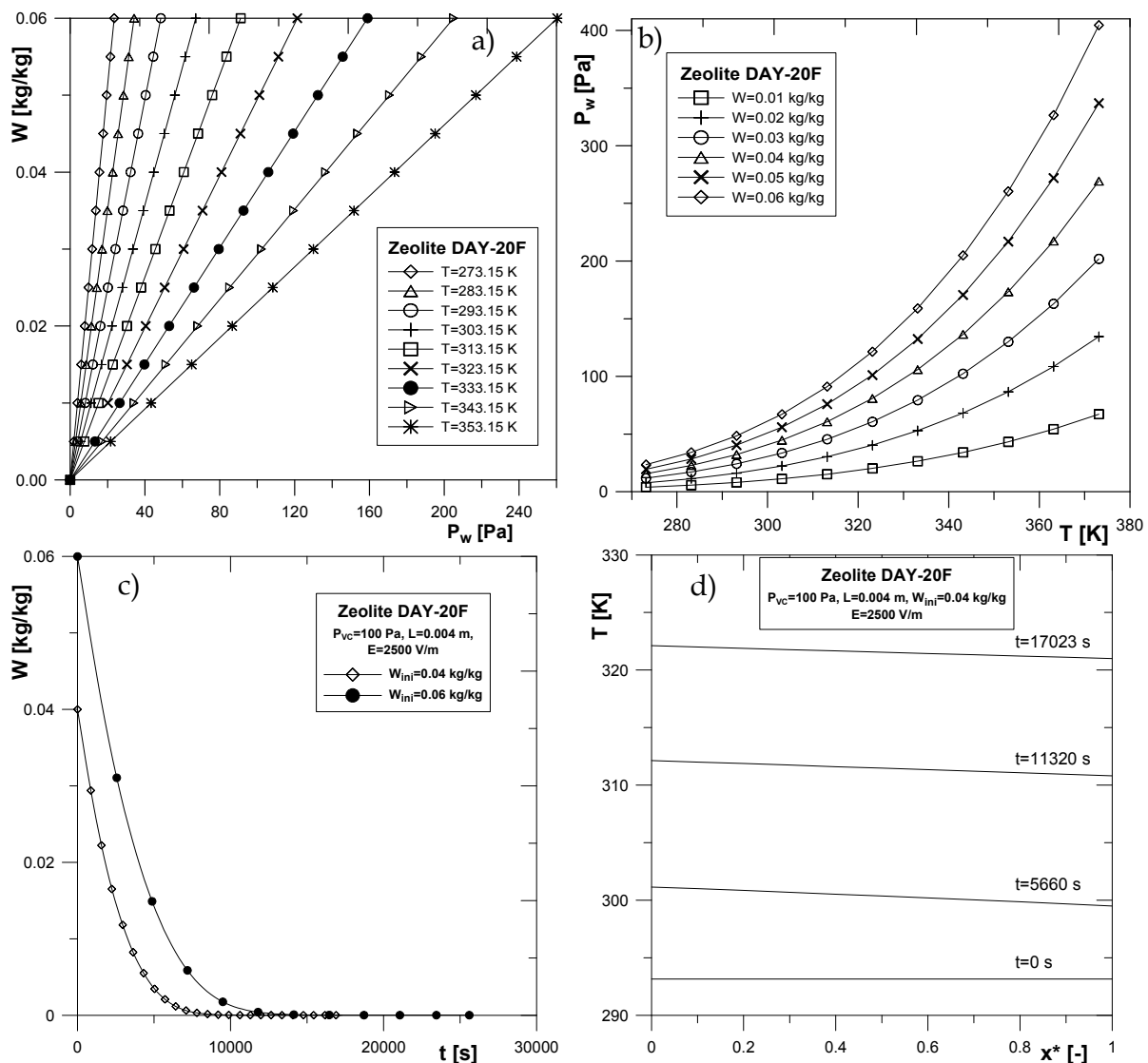


Fig. 9. Exemplary simulation of Zeolite DAY-20F secondary MFD: a) multitemperature adsorption isotherms and b) isosteres of water vapor; c) drying curves; d) temperature profiles in the sample for various process times.

Multitemperature Langmuir isotherm of water vapor on Zeolite DAY-20F in wide range of pressure is shown in Figure 9a. Additionally multitemperature Langmuir isostere for the same system is depicted in Figure 9b. Physical properties of Zeolite DAY-20F assumed at average bed temperature 303.15 K and process pressure 100 Pa are as follows:  $k_{eII} = 0.025$  W/(mK),  $c_s = 900$  J/(kgK),  $\rho_{buII} = 500$  kg/m<sup>3</sup>;  $\varepsilon = 0.677$ .

During the primary freeze drying stage equilibrium water vapor pressure in region II equals approximately vapor pressure at sublimation front, i.e. 100 Pa. Equilibrium material (Zeolite DAY-20F) moisture content relative to that pressure equals about 0.05 kg/kg for maximal material temperature: 323 K (Fig. 9b). Thus for dried layer temperatures range (region II), taking place during primary freeze drying (below 323 K) moisture desorption does not exist. Formulated here mathematical model of the secondary vacuum freeze drying at microwave heating consisting of equations (56)-(59) with adequate initial and boundary conditions (53,

54) was solved by 4th order Runge-Kutta method with the following process parameters:  $L=0.004$  m,  $W_{ini}=0.04$  or  $0.06$  kg/kg,  $\mu_{1II} = 1.107 \times 10^{-6}$  W/(mV<sup>2</sup>K),  $\mu_{2II} = 1.021 \times 10^{-3}$  W/(mV<sup>2</sup>),  $E = 2500$  V/m and initial bed temperature  $T(x,0) = 293.15$  K. Calculated dissipation coefficient at this conditions amounts to  $K_{dissII} = 1.054 \times 10^{-3}$  and average capacity of internal volumetric heat source throughout the material equals:  $Q_v = 6588$  W/m<sup>3</sup>. Obtained results of numerical simulation are presented in Figs. 9c and 9d. Moisture contents versus time for two initial bed moisture contents  $W_{ini} = 0.04$  and  $0.06$  kg/kg in Zeolite DAY-20F bed of thickness  $L = 0.04$  m are shown in Figure 9c. Figure 9d depicts dried bed temperatures versus dimensionless positions in the material layer, for various process times at sample thickness  $L = 0.04$  m and initial moisture content  $W_{ini} = 0.04$  kg/kg.

## 5. Conclusions

The mathematical model of both the primary and the secondary freeze drying stages of random solids at microwave heating was developed. Experimental and/or theoretical investigations of the primary freeze drying at microwave heating were presented for three selected materials: beef, Sorbonorit 4 activated carbon and mannitol. Furthermore, theoretical analysis of the secondary freeze drying at microwave heating was performed for Zeolite DAY-20F bed.

For dried granular materials such as: Sorbonorit 4, Zeolite DAY-20F, characterized by considerable internal porosity, primary freeze drying stage is not sufficient to remove entire moisture contained in the dried bed. During the primary freeze drying at microwave heating free, interstitial moisture is removed. The secondary freeze drying stage is then necessary to remove residual moisture which may be as high as 7%, after primary stage.

Kinetics of the microwave freeze drying process is enhanced in comparison with the freeze drying at conventional heating. It is caused mainly by the fact, that in conventional heating (e.g. contact or radiative) temperature and mass transfer gradients in the dried material have opposite directions. On the contrary, in the freeze drying process at microwave heating both temperature, and mass transfer gradients are cocurrent. It is very convenient phenomenon from point of view of the qualitative final dried material properties.

Assumption of constant electric field strength in a dried material is valid for sample dimensions up to half wavelength order in monomodal resonant cavities. Formulated mathematical model can be also applicable in the microwave heating of sample dimensions equaled multiple of wavelengths in multimodal applicators with uniform distribution of electric field strength.

The model for the secondary freeze drying at microwave heating takes into account mass transfer resistances which arise in vacuum desorption. The LDF mass transfer model with a variable, lumped-resistance coefficient  $K$  was used. This numerical model was applied to perform computer simulation of the vacuum desorption of pure water from Zeolite DAY-20F.

Experimental verification of the some model simulations of the primary freeze drying at microwave heating approved its fairly good usefulness for design applications. Furthermore, mathematical model of the vacuum desorption in the secondary freeze drying enables predictions of the drying kinetics for the granular solids.

## 6. Nomenclature

$a_e$	effective thermal diffusivity (m <sup>2</sup> /s)
$c_p, c_{pw}$	effective specific heat (material region, water vapor) (J/kg K)
$c_{pg}$	effective specific heat of gas phase (J/mol K)
$C$	gas phase molar concentration (mol/m <sup>3</sup> )
$C_w, C_{s,3}$	water vapor mass concentration (general, triple point) (kg/m <sup>3</sup> )
$d_e$	equivalent particle diameter (m)
$D_{eII}, D_K, D_M, D_S$	water vapor diffusivity (effective, Knudsen, molecular, surface) in dry layer (m <sup>2</sup> /s)
$E, E, E_0, E_{rms}$	electric field strength (general, spatial vector, peak, r.m.s.) (V/m)
$f$	frequency (Hz)
$K_{diss}$	dissipation coefficient (W/mV <sup>2</sup> )
$L$	sample thickness (m)
$M_w, M_{in}$	molar mass (water, inert) (kg/mol)
$N$	gas phase molar flux density in the secondary MFD (mol/m <sup>2</sup> s)
$N_w$	water vapor mass flux density from sublimation front (kg/m <sup>2</sup> s)
$P$	total pressure (Pa)
$q$	heat flux density (W/m <sup>2</sup> )
$Q_v$	volumetric heat source capacity (W/m <sup>3</sup> )
$r_p$	mean pore radius (m)
$R$	universal gas constant (J/mol K)
$t$	time (s)
$T, T_{II_{avg}}, T_{s,3}, T_0$	temperature (general, average in region II, triple point, starting value) (K, °C)
$W, W_{eq}, W_{ini}, W_0$	moisture content of dried bed (average, equilibrium, initial, starting value when microwave heating is turned on) (dry basis, kg/kg)
$x, X, X_0$	Cartesian position coordinate (general, moving boundary, starting) (m)
$y_w, y_{w_{eq}}$	water vapor mole fraction (general, equilibrium) (mol/mol)
Greek symbols	
$\alpha_{II\infty}$	heat transfer coefficient at the surface of dried region II (W/m <sup>2</sup> K)
$\delta$	arbitrary initial thickness of the dried layer (m)
$\tan \delta$	dielectric loss tangent (-)
$\Delta h_s$	enthalpy of sublimation (J/kg)
$\Delta h_{ads}$	heat of adsorption (J/mol)
$\varepsilon$	bed porosity, (-)
$\varepsilon_0$	free space permittivity (F/m)
$\varepsilon'$	relative dielectric constant (-)
$\varepsilon''$	relative loss factor (-)
$\eta$	gas phase viscosity (Pa s)
$\lambda_0, \lambda_w$	wavelength (free space, waveguide) (m)
$\mu_1$	constant in Eq. (8) (W/mV <sup>2</sup> K)
$\mu_2$	constant in Eq. (8) (W/mV <sup>2</sup> )

$\rho_{bu}$  bulk density (kg/m<sup>3</sup>)  
 $\omega$  angular frequency (rad/s)

Subscripts and superscripts

1, 2 gas phase (water vapor, air)  
I, II region number (frozen, dried)  
L at sample exposed surface  
s at moving boundary (sublimation front)  
vc vacuum chamber  
\* dimensionless value

Abbreviations

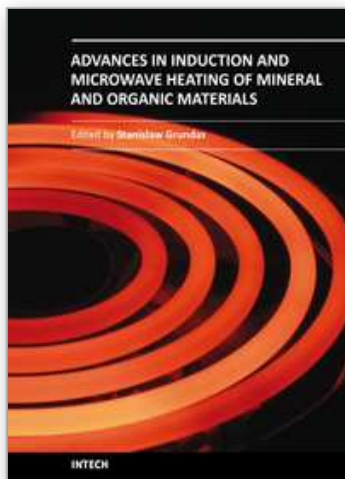
FD freeze drying  
LDF linear driving force  
LT Landau transformation  
MB moving boundary (sublimation front)  
MFD microwave freeze drying  
NMOL numerical method of lines  
VTS variable time-step

## 7. References

- Ang, T.K.; Ford, J.D. & Pei, D.C.T. (1977). Microwave freeze-drying of food: a theoretical investigation, *International Journal of Heat and Mass Transfer*, 20, pp. 517-526.
- Chahbani, M.H. & Tondeur, V. (2001). Pressure drop in fixed-bed adsorbers, *Chem. Eng. J.*, 81, pp. 23-34.
- Coulson, J.M.; Richardson, J.F. & Sinnott, R.K. (1999). *Chemical Engineering*, Vol. 6, Butterworth-Heinemann, Oxford.
- Do, D.D. (1998). *Adsorption Analysis: Equilibria and Kinetics*, Imperial College Press, London.
- Ergun, S. (1952). Fluid flow through packed column, *Chem. Eng. Progress*, 48, pp. 89-94.
- Glueckauf, E. (1955). Theory of chromatography, *Trans. Faraday Soc.*, 51, pp. 1540-1551.
- Liapis, A.I. & Bruttini R. (1996). Mathematical models for the primary and secondary drying stages of the freeze drying of pharmaceuticals on trays and vials. In: *Mathematical Modeling and Numerical Techniques in Drying Technology*, Turner, I & Mujumdar, A.S., (Eds), pp. 481-536, CRC Press, ISBN: 9780824798185, Marcel Dekker, New York.
- Liapis, A.I. & Bruttini, R. (2006). Freeze drying, In: *Handbook of Industrial Drying*, Mujumdar A.S., (Ed.), pp. 257-284, CRC Press, ISBN: 9781574446685, New York.
- Ma, Y.H. & Peltre, P.R. (1973). Mathematical simulation of a freeze drying process using microwave energy, *AIChE Symp. Ser.*, 132, 69, 47-54.
- Ma, Y.H. & Peltre, P.R. (1975a). Freeze dehydration by microwave energy: Part I. Theoretical investigation. *AIChE Journal*, 21, 2, pp. 335-344.
- Ma, Y.H. & Peltre, P.R. (1975b). Freeze dehydration by microwave energy: Part II. Experimental Study. *AIChE Journal*, 21, 2, pp. 344-350.
- Metaxas, A. C. (1996). *Foundations of Electroheat: A Unified Approach*, John Wiley & Sons, New York.

- Péré, C.; Rodier, E. & Louisnard, O. (2001). Microwave vacuum drying of porous media: verification of a semi-empirical formulation of the total absorbed power. *Drying Technology*, 19, 6, pp. 1005-1022.
- Poling, B.E.; Prausnitz, J.M. & O'Connell, J.P. (2001). *The properties of gases and liquids*, Fifth Edition, McGraw-Hill, New York.
- Rowe, T.W. & Snowman, J.W. (1978). *Edwards Freeze drying Handbook*, Crawley, Cambridge.
- Schiesser, W.E. (1991). *The Numerical Method of Lines: Integration of Partial Differential Equations*, Academic Press, New York.
- Schiffmann, R.F. (2006). Microwave and dielectric drying. In.: *Handbook of Industrial Drying* Mujumdar A.S., (Ed.), pp. 286-306, CRC Press, ISBN: 9781574446685, New York.
- Sun, L.M.; Amar, N.B. & Meunier F. (1995). Numerical study on coupled heat and mass transfer in an adsorber with external fluid heating, *Heat Recovery Systems & CHP*, 15, pp. 19-29.
- Wang, Z.H. & Shi, M.H. (1998). Numerical study on sublimation-condensation phenomena during microwave freeze drying. *Chemical Engineering Science*, 53, 18, pp. 3189-3197.
- Wang, W. & Chen, G. (2003). Numerical investigation on dielectric material assisted microwave freeze-drying of aqueous mannitol solution. *Drying Technology*, 21, 6, pp. 995-1017.
- Witkiewicz, K. (2006). *The Numerical Modeling of Freeze Drying of Granular Solids at Microwave Heating*, Ph.D. Dissertation, Szczecin University of Technology, Szczecin, (in Polish).
- Wolff, E.; Gilbert, H. & Rodolphe, F (1989). Vacuum freeze drying kinetics and modelling of a liquid in a vial, *Chemical Engineering and Processing*, 25, pp. 153-158.
- Yuen, W.W. & Kleinman, A.M. (1980). Application of a variable time-step finite-difference method for the one-dimensional melting problem including the effect of subcooling, *AIChE Journal*, 26, 5, pp. 828-832.
- Yun, J.-H.; Choi, D.-K. & Kim, S.-H. (1999). Equilibria and dynamics for mixed vapors of BTX in an activated carbon bed, *AIChE. Journal*, 45, 4, pp. 751- 760.

IntechOpen



## **Advances in Induction and Microwave Heating of Mineral and Organic Materials**

Edited by Prof. Stanisław Grudas

ISBN 978-953-307-522-8

Hard cover, 752 pages

**Publisher** InTech

**Published online** 14, February, 2011

**Published in print edition** February, 2011

The book offers comprehensive coverage of the broad range of scientific knowledge in the fields of advances in induction and microwave heating of mineral and organic materials. Beginning with industry application in many areas of practical application to mineral materials and ending with raw materials of agriculture origin the authors, specialists in different scientific area, present their results in the two sections: Section 1-Induction and Microwave Heating of Mineral Materials, and Section 2-Microwave Heating of Organic Materials.

### **How to reference**

In order to correctly reference this scholarly work, feel free to copy and paste the following:

Józef Nastaj and Konrad Witkiewicz (2011). Experimental and Simulation Studies of the Primary and Secondary Vacuum Freeze Drying at Microwave Heating, *Advances in Induction and Microwave Heating of Mineral and Organic Materials*, Prof. Stanisław Grudas (Ed.), ISBN: 978-953-307-522-8, InTech, Available from: <http://www.intechopen.com/books/advances-in-induction-and-microwave-heating-of-mineral-and-organic-materials/experimental-and-simulation-studies-of-the-primary-and-secondary-vacuum-freeze-drying-at-microwave-h>

**INTECH**  
open science | open minds

### **InTech Europe**

University Campus STeP Ri  
Slavka Krautzeka 83/A  
51000 Rijeka, Croatia  
Phone: +385 (51) 770 447  
Fax: +385 (51) 686 166  
[www.intechopen.com](http://www.intechopen.com)

### **InTech China**

Unit 405, Office Block, Hotel Equatorial Shanghai  
No.65, Yan An Road (West), Shanghai, 200040, China  
中国上海市延安西路65号上海国际贵都大饭店办公楼405单元  
Phone: +86-21-62489820  
Fax: +86-21-62489821

© 2011 The Author(s). Licensee IntechOpen. This chapter is distributed under the terms of the [Creative Commons Attribution-NonCommercial-ShareAlike-3.0 License](#), which permits use, distribution and reproduction for non-commercial purposes, provided the original is properly cited and derivative works building on this content are distributed under the same license.

IntechOpen

IntechOpen